Preprints (www.preprints.org) | NOT PEER-REVIEWED | Posted: 11 March 2022 doi:10.20944/preprints202203.0167.v1

Article

Microstructural parameters for modelling of superconducting foams

Michael Rudolf Koblischka [1],Anjela Koblischka-Veneva [1], Quentin Nouailhetas[1,2], Ghazi Hajiri[2], Kévin Berger[2], Bruno Douine[2], Denis Gokhfeld[3]

[1] Saarland University, Experimental Physics, P. O. Box 151150, D-66041 Saarbrücken, Germany.
[2] Université de Lorraine, GREEN, F-54000 Nancy, France.
[3] Federal Research Center KSC SB RAS, Kirensky Institute of Physics, Krasnoyarsk, 660036 Russia.
* Correspondence: m.koblischka@gmail.com

Abstract: Superconducting $YBa_2Cu_3O_y$ (YBCO) foams were prepared using commercial open-cell, polyurethane foams as starting material to form ceramic Y_2BaCuO_5 (Y-211) foams which are then converted into superconducting YBCO by using the infiltration growth process. For modelling the superconducting and mechanical properties of the foam samples, a Kelvin-type cell may be employed as a first approach as reported in the literature for pure polyurethane foams. However, for a refined model of a superconducting foam sample, the real sample structure must be considered. Thus, a proper description of the specific microstructure of the superconducting YBCO foams is required. A variety of parameters including the cell size and shape, the window size and shape, the length and shape of the foam struts or ligaments and the respective angles of intersection were used to describe the real foam structure. To obtain a set of reliable data, YBCO foam samples were investigated using optical microscopy, scanning electron microscopy and electron backscatter diffraction (EBSD). A detailed investigation of the foam microstructure revealed not only the differences to the polymeric foams used as base material, but also provided insight into the infiltration growth process via the increased surface amount in a foam sample.

Keywords: Superconducting foams, YBCO, microstructure, modelling parameters, foam cells, current flow

check for updates

Citation: Koblischka, M. R.; Koblischka-Veneva, A.; Nouailhetas, Q.; Hajiri, G.; Berger, K.; Douine, B.; Gokhfeld, D. Microstructural parameters for modelling of superconducting foams. *Preprints* **2021**, *1*, 0. https://doi.org/

Received:
Accepted:
Published:

Publisher's Note: MDPI stays neutral with regard to jurisdictional claims in published maps and institutional affiliations.

1. Introduction

Superconducting $YBa_2Cu_3O_y$ (YBCO) open-cell foam samples [1–3] are interesting materials for a variety of applications (fault current limiters, trapped field magnets, space applications [4–10]) due to their various, unique properties, which include low sample weight, a very effective oxygenation process, excellent thermal properties allowing for quick cooling, excellent mechanical properties, the possibility for easy shaping of the samples and straightforward upscaling of the sample size. The cooling effectivity, effective oxygenation and sample upscaling have previously been demonstrated in [3,11,12]. Measurements of trapped fields (TFs) in superconducting YBCO foam samples [12–14] have revealed a more complicated TF pattern than those of conventional bulk samples. The presence of several small peaks in the TF patterns was ascribed to the compression of local current loops in the sample. Furthermore, it was found that these small peaks do not arise from the same positions in the sample for subsequent TF experiments. These observations demonstrated that current flow through a superconducting foam sample is complicated due to the 3D arrangement of the foam struts, so that local current loops can be formed. Another observation is that the mechanical strength of the foam samples is superior to that of conventional samples. The foams are less prone to cracking caused by magnetostriction [15,16]. The typical internal cracks of bulk samples due to the oxygenation process [17,18] do not exist in the foams.

Thus, to enable the use of superconducting foam samples in various applications, a better understanding of their superconducting and mechanical properties is essential. Computer modelling may be used to assist in reaching this goal. This approach has been utilized in delineating the mechanical and thermal properties of polymer and metal foam

© 2022 by the author(s). Distributed under a Creative Commons CC BY license.

Preprints (www.preprints.org) | NOT PEER-REVIEWED | Posted: 11 March 2022 doi:10.20944/preprints202203.0167.v1

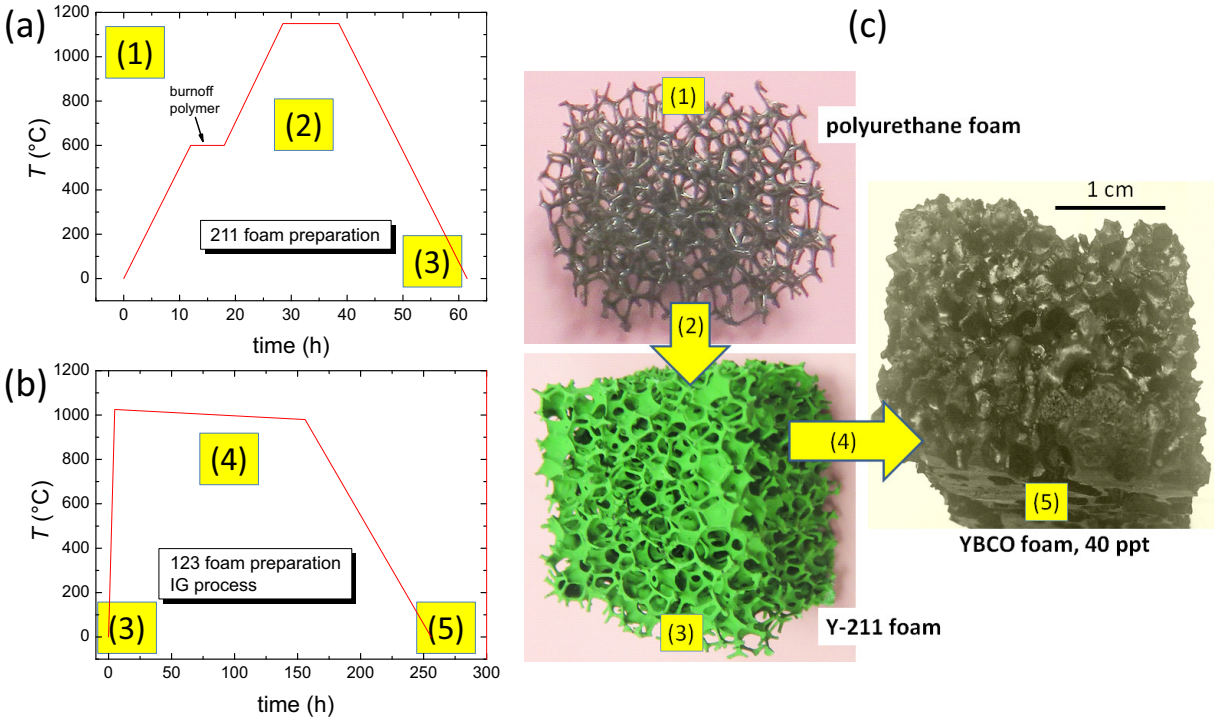

Figure 1. (**a**) Heat treatment to obtain the Y211 foam, (**b**) heat treatment (IG-process) converting the Y-211 foam to an superconducting YBCO foam. (**c**) Illustration of the foam samples at different process stages (1), (3) and (5).

materials [19–24].

The already existing modelling approaches for polyurethane foams [20–24] may provide a useful starting point. It has been shown that modelling of foam samples with a regular succession of cells and a simple cell geometry (the Kelvin cell) as a first approximation does permit reasonable prediction of properties. However, for a better description of the mechanical properties of polymer and metallic foam materials [25–30], it is necessary to improve the model using parameters from the real foam structure. Therefore, it is essential to properly evaluate the microstructure of the superconducting foams to obtain information to improve the modelling. This is particularly important since the double-step fabrication process (polyurethane foam → ceramic Y_2BaCuO_5 (Y-211)-foam → superconducting YBCO foam) may alter the original foam microstructure. Although to a first approximation, the ceramic material will mimick the structural arrangement of the polymer foam. Furthermore, the infiltration growth process [31,32] applied to the foam sample will create an unique microstructure which is not seen in bulk superconductors [33] due to the large amount of internal surfaces in the foam structure.

To achieve a better understanding of the details of the foam microstructure, a thorough analysis of the real foam microstructure of open-cell, superconducting YBCO foams has been performed. Digital optical microscopy, scanning electron microscopy (SEM) and electron backscatter diffraction (EBSD) have been used to identify the structural parameters important for modelling of superconducting foam samples.

2. Experimental procedures

2.1. Sample preparation

For better understanding the microstructure of the superconducting YBCO foams, the details of the fabrication steps must be considered. The preparation process of the superconducting YBCO foam samples is a two-step process:

Preprints (www.preprints.org) | NOT PEER-REVIEWED | Posted: 11 March 2022 doi:10.20944/preprints202203.0167.v1

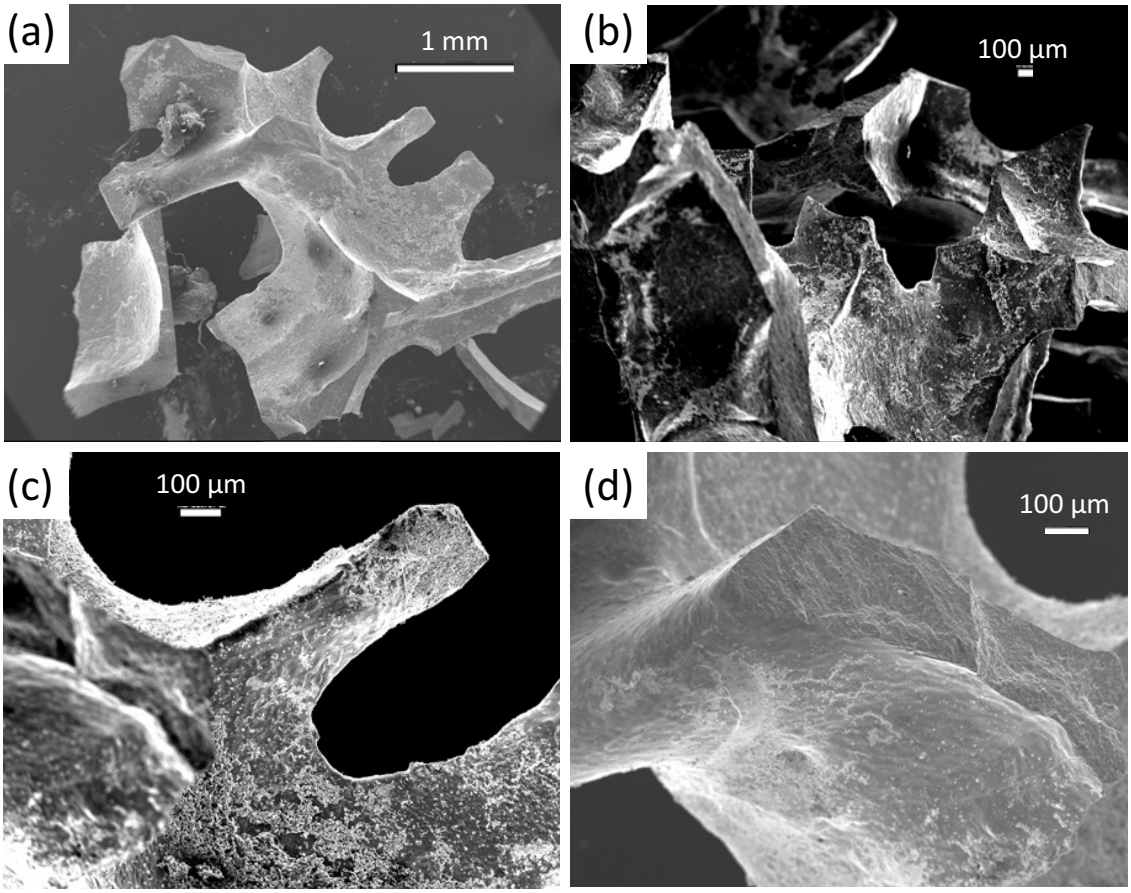

Figure 2. (**a-d**) SEM images at low magnification of broken-out foam strut pieces from a superconducting YBCO foam, giving information of the real foam microstructure and the various internal surfaces existing in the open-cell foam structure. Note the rough character of the as-grown strut surfaces of the YBCO foam. The images further demonstrate the irregular shape and size distribution of the foam struts, which need to be modelled.

(i) Starting from commercially available polyurethane foams (1), which define the porosity of the final product, the sample is covered with a slurry of Y-211 powder dissolved in polyvinyalcohol (PVA) and water. To form ceramic Y-211 foams, a heat treatment is required to burn off the polyurethane and to compact the Y-211 ceramic (2). This is illustrated in the temperature program shown in Fig. 1 (a).

(ii) The green Y-211 foam (3) is then converted into the YBCO superconductor using the infiltration growth process [31,32] using a Nd-123 seed crystal on top and a liquid source consisting of a 1:1 mixture of Ba and Cu oxides with an overall stoichiometry of $Ba_3Cu_5O_y$ and additional 123 powder placed beneath the Y-211 foam. When being heated above the eutectic temperature (1010 °C, (4)), the liquid phase infiltrates the Y-211 foam by capillary action [34]. Finally, the Y-211 foam is fully converted to the 123-phase (5) in a slow-cooling process.

Thus, the superconducting YBCO foams owe their specific properties to the IG process applied. The liquid phase, which moves along the foam struts from bottom to the top of the sample, plays an essential role for the appearance and shape of the foam struts. This will be investigated in detail using electron microscopy and digital optical microscopy in the following sections. The samples investigated in this study were prepared at RWTH Aachen, Germany, as well as new ones, which were fabricated using the same process parameters.

Preprints (www.preprints.org) | NOT PEER-REVIEWED | Posted: 11 March 2022 doi:10.20944/preprints202203.0167.v1

2.2. Microscopy investigations

Digital optical microscopy was performed using a Keyence VHX-5000 microscope [35] with large depth of field and long observation distance (most images were taken with 100× magnification), enabling 3D imaging and digital image processing/analysis. The images were treated by the built-in analysis software for calibration and size measurements. Using the possibility to record the image processing steps, an automated routine for determining, e.g., the window sizes, can be generated. This enables a large number of images to be processed in reasonable time. Additional image analysis was performed using ImageJ [36] and WSxM software [37].

SEM images were taken using a field emission scanning electron microscope (JEOL 7600 F) and a JEOL 7000F SEM microscope operating at 20 kV with a working distance of 10 mm. EDX analysis was performed using a EDAX ZAF system with a SUTW sapphire detector.

The EBSD orientation imaging was performed in a JEOL 7000F SEM microscope equipped with a TSL (TexSEM Labs, UT [38]) analysis unit. The Kikuchi patterns were generated in reflection mode [39] at 15 kV, and were recorded by means of a DigiView camera system. To perform crystallographic orientation mapping, the electron beam was scanned over a selected surface area and the resulting Kikuchi patterns were indexed and analyzed automatically. Automated EBSD scans were performed with an EBSD step size down to 50 nm.

The sample surfaces for EBSD analysis were mechanically polished using SiO_2 grinding papers, followed by mechanical polishing with diamond pastes (3 μm down to 1/4 μm diamonds) using ethanol as lubricant. The final step consisted of polishing the surface using colloidal silica with 40 nm particles (Struers OP-S solution). More details on the sample surface preparation steps can be found in [40]. An additional low-angle (5°) Ar ion-polishing step (5 keV, 5 min) could be applied to the sample surface after the mechanical treatment. This process increases the image quality (IQ) of the resulting Kikuchi patterns and removes mainly adhered particles on the sample surface.

3. Results and discussion

3.1. Scanning electron microscopy

Figures 2 (a)-(d) present SEM images in various magnifications of foam strut pieces broken-out from a bulk YBCO foam. These pieces reveal the directly the complicated and irregular arrangement of the foam struts and their vertices within the foam sample (a,b), exhibiting various ligament (strut) lengths, ligament cross sections and intersection angles. In the following, a foam strut denotes an entire broken-out section and the ligament is the material section between two adjacent nodes. In case of higher magnification (c,d), the images reveal further a certain characteristic structure of the foam strut surface. This structure was caused by the capillary flow of the liquid phase along the Y-211 struts, which left a rough and rugged surface, comprising several particles, particle clusters and flow structures. In Figs. 3 (a)-(c), more details of the strut surface structure are presented using higher magnification, illustrating the distribution of the $Ba_3Cu_5O_y$ particles. Here, it must be noted that the foam sample offers a high amount of internal surfaces, which do not exist in conventional bulk samples prepared using the same IG-processing method. The images 3 (a)-(c) reveal that a large number of $Ba_3Cu_5O_y$ particles with typical size ranging between 0.5 and 3 μm are distributed in an irregular fashion on the strut surfaces as individual particles or as particle clusters. EDX analysis (d) revealed that the particles are mainly $Ba_3Cu_5O_y$, that is, particles of the pure liquid phase used in the IG-processing. Besides these particles, the SEM images indicate distinct growth steps and some characteristic patterns on the strut surfaces, which are caused by the capillary flow of the liquid phase. These patterns were shown by EDX to possess a higher content of Y as the particles on the surface. All this information gained on the strut surfaces gives valuable input to better understand the details of the IG-process, which are not seen in conventional bulk samples.

Preprints (www.preprints.org) | NOT PEER-REVIEWED | Posted: 11 March 2022 doi:10.20944/preprints202203.0167.v1

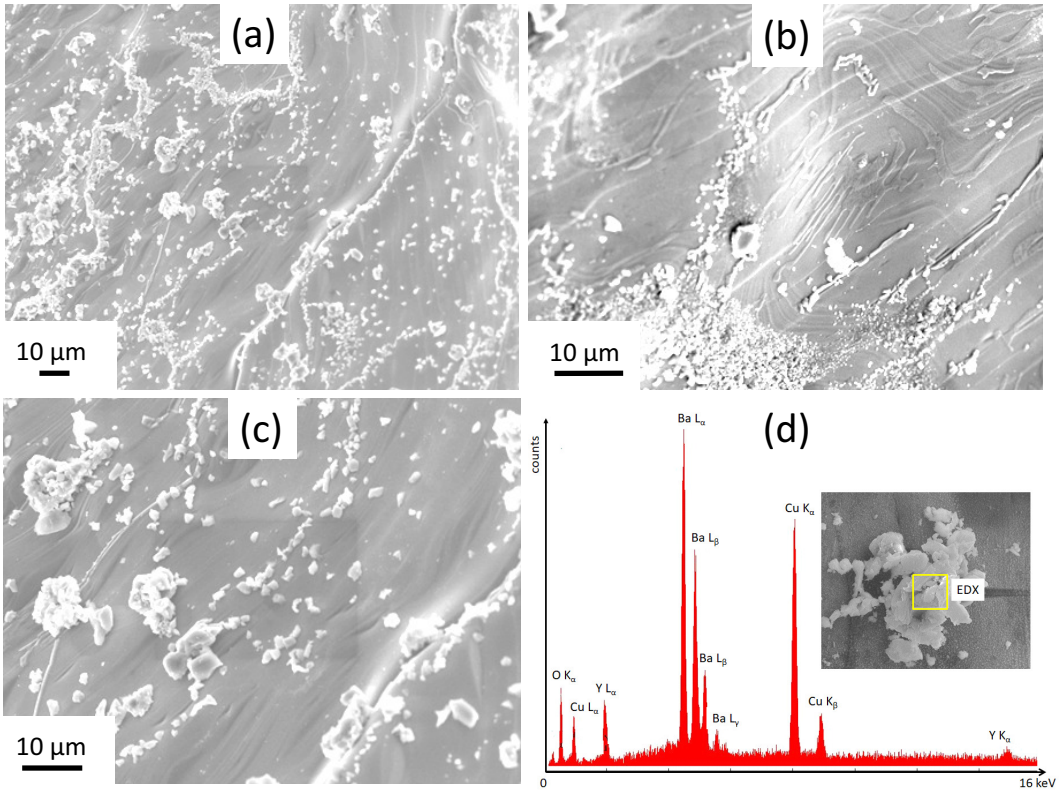

Figure 3. (**a-c**) SEM images (various magnifications) showing details of the internal surfaces of the foam struts and vertices. The particles seen on the strut surfaces are $Ba_3Cu_5O_y$ particles as determined by EDX analysis (**d**). These structures and particles are caused by the capillary flow of the liquid phase during IG-processing, which is not seen in conventional bulk samples.

A closer investigation of these particles on the strut surfaces and their possible effect on the flux pinning properties will be presented in a forthcoming study [41].

Figures 4 (a)-(c) present EBSD measurements on polished foam strut surfaces. Figure 4 (a) is an overview measurement of the orientation distribution (inverse pole figure, abbreviated IPF) in [001]-direction along a foam strut ligament. The scan area is selected to be fully *inside* the foam strut. Furthermore, as the strut surface has underwent mechanical polishing, the particles on the surface are removed, so only 2 phases (YBCO and Y-211) are present. The crystallographic orientations are given perpendicular to the sample surface, i.e., in [001]-direction. Note that there is practically no orientation in [001]-direction (red) like in the case of a bulk superconductor pellet, which is due to the original 3D orientation of the strut *within* the bulk foam. Thus, the present observation is *not* contradicting the overall texture of the bulk foam as verified by neutron diffraction in [42,43]. The YBCO matrix consists of elongated grains showing various orientations 30-60° off the [001]-orientation. In contrast, the large Y-211 particles seem to be randomly oriented. In Figs. 4 (b) and (c), EBSD-mappings with high resolution are shown using an EBSD stepsize of 50 nm. Figure 4 (b) presents a phase map with YBCO plotted in red and Y-211 in green. Furthermore, the EBSD-detected grain boundaries (GBs) are marked by thin black lines. There are several large Y-211 particles showing some substructures. Many small grains are located along the edges of the big Y-211 grains, but also very tiny Y-211 particles covering just one EBSD step [44] can be detected. This is indication of a small particle size $\sim$ 50 nm. Large numbers of such tiny Y-211 particles are found to fill the GBs between the YBCO grains (yellow arrows point to several such locations). This type of arrangement of Y-211 particles was not observed in any bulk YBCO pellets as already discussed in [45]. The inverse pole figure (IPF) orientation map, overlaid with the image quality (IQ) information, presented in Fig. 4

Preprints (www.preprints.org) | NOT PEER-REVIEWED | Posted: 11 March 2022 doi:10.20944/preprints202203.0167.v1

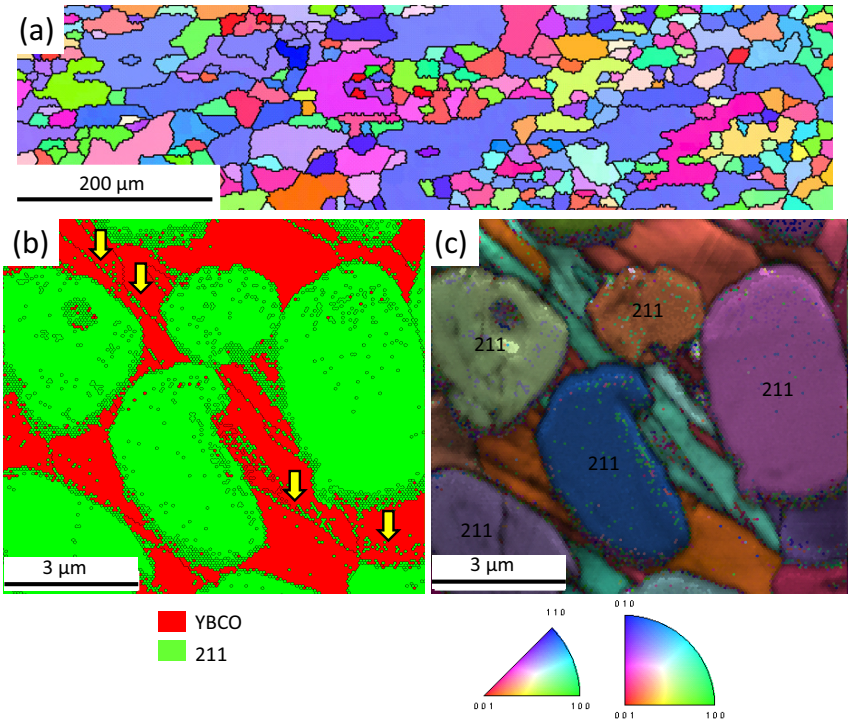

Figure 4. (**a-c**) EBSD orientation imaging of foam strut pieces with mechanically polished surfaces. The scan areas are selected to be entirely inside the struts. (**a**) Overview measurement (scan area ∼ 1 mm × 200 μm) along a foam strut ligament. Orientations are given perpendicular to the sample surface, i.e., in [001]-direction. The EBSD stepsize for this measurement was 2 μm. Both phases (YBCO and Y-211) are plotted together. The color code for the orientation mapping is given below image (**c**). (**b**) Phase mapping (red – YBCO, green – Y-211) of a 10 × 10 μm^2 scan area. Several large and many tiny Y-211 particles are embedded within the YBCO matrix. The EBSD-detected GBs are indicated using thin, black lines. The yellow arrows point to the tiny Y-211 particles found in groove-like structures in the foam strut. (**c**) Inverse pole figure (IPF) map with overlaid image quality (IQ) mapping, recorded with high magnification and an EBSD stepsize of 50 nm. Note here that the YBCO matrix shows orientations up to 60° off the [001]-orientation which reflects the 3D-orientation of the strut within the bulk foam. The Y-211 particles reveal several different orientations.

(c) reveals that only two main orientations exist for the YBCO grains within the scanned area. In contrast, the large Y-211 grains are practically randomly oriented.

All observations of grain orientations within the foam struts are important to understand the flow of superconducting currents in the superconducting foam samples. Most importantly, the EBSD data reveal that the currents within a foam strut must cross several GBs, which poses a severe limitation as seen in the time-dependent TF measurements performed in [46], even though the overall foam sample has texture introduced by the seed crystal, which was verified by neutron diffraction experiments [42,43]. The possible influence of the $Ba_3Cu_5O_y$ particles located on the strut surfaces on the flux pinning properties was not yet studied, but it is obvious that the capillary transport of the liquid phase along the foam struts has altered the shape and appearance of the final YBCO foam struts as compared to those of the polyurethane foams, from which the processing had started.

3.2. Digital optical microscopy

Using digital optical microscopy, a large number of images were taken to study the various shapes of the cells building up the YBCO foam sample. Using the specific focal depth variation enabled to obtain processed 3D images of the foam cells. All the images presented here were collected on full-size foam samples by means of a Keyence VHX-5000 microscope. The included image analysis software enabled a semi-automated analysis.

Preprints (www.preprints.org) | NOT PEER-REVIEWED | Posted: 11 March 2022 doi:10.20944/preprints202203.0167.v1

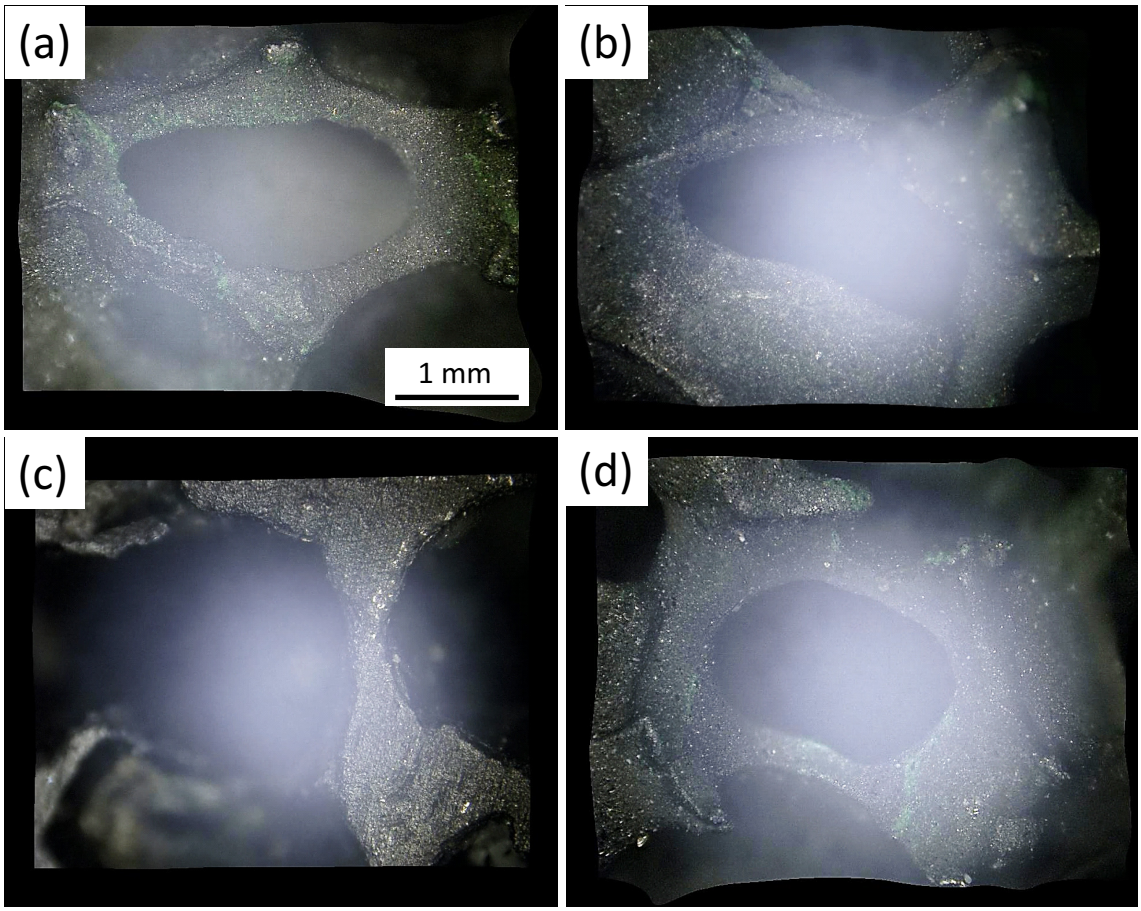

Figure 5. (**a-d**) Optical raw images of foam struts, ligaments and windows in various positions within the bulk foam sample taken by a Keyence VHX-5000 microscope, allowing a large focal depth. These images provide an impression of the local variation of the foam windows, struts and ligaments, which need to be modelled.

Overall, about 200 such images were collected and analyzed. Figures 5 (a)-(d) present untreated raw images of several foam cells with a high focal depth, showing typical foam struts and windows in their original location within the foam sample. These images serve as the input for the following analysis. The image-processed images of the foam microstructure as shown in Figs. 6 (a)–(f) give an impression of the real arrangement of the foam struts, windows and cells. This analysis provides the necessary input data (ligament length, intersection angles and window size) to the statistical analysis to obtain proper parameters for the modelling.

3.3. Discussion of modelling approaches and parameters

The first issue is a discussion about the sample density and the amount of superconducting material in a foam sample. As the superconducting foams are prepared via the IG-process, the foam struts share their properties with the IG-processed bulks, even though there are certain differences in the microstructure. In [10], the densities of various melt-processed samples was discussed leading to different levitation forces. The density of the melt-textured samples ranged between 5.88 and 6.17 g/cm^3, the tabulated theoretical density of YBCO being 6.4 g/cm^3. The difference is due to the presences of pores and cracks, and also the lower density of Y-211 particles which make up to 40% of the material. In the case of foams, the presence of pores reduces the density to 1/5...1/10 of the density of the bulks, depending on the porosity of the original polyurethane foam (20...40 ppi).

The previous modelling of polyurethane foams clearly revealed that it is important to properly model the real foam microstructure in order to achieve reasonable results for the mechanical properties of such foams as the real foam samples showed higher mechanical

Preprints (www.preprints.org) | NOT PEER-REVIEWED | Posted: 11 March 2022 doi:10.20944/preprints202203.0167.v1

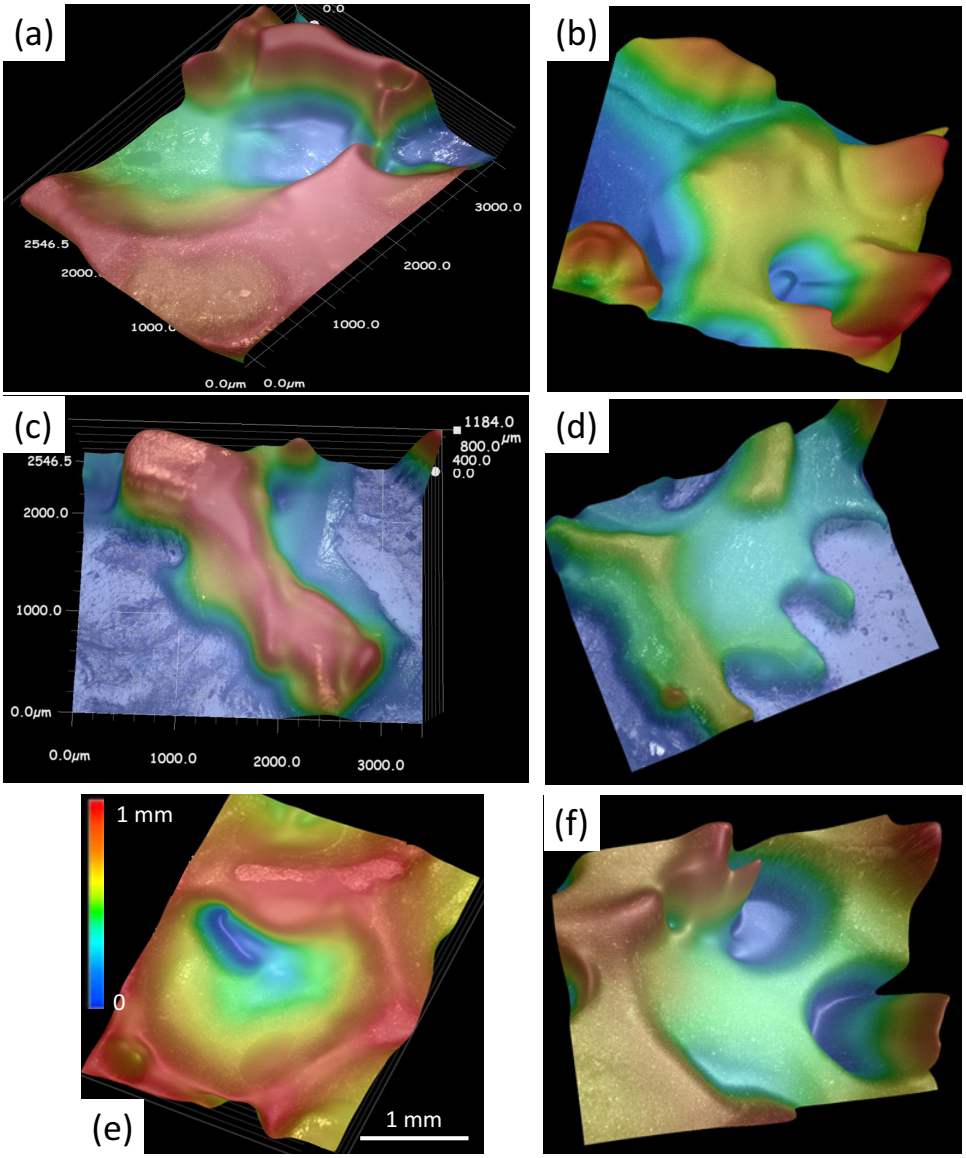

Figure 6. (**a-f**) Digitally processed images of foam windows, struts and ligaments in various positions within the bulk foam sample. Images (a) and (c) show the calibrated size data, and (e) gives the extracted values for x and the color code for z. These images are the base for the analysis presented in Fig. 7 below.

strength. Thus, we have analyzed about 200 such images to obtain a reasonable parameter set characterizing the YBCO foam samples.

Figure 7 (a) presents the definition of the ligament length (orange line), the intersection angle α (red lines) and the foam windows (yellow ellipses). Ligament lengths and intersection angles were determined manually, whereas the window size was determined via the Keyence software with selected border values.

The Kelvin cell geometry has already been used by many researchers to represent foam structures [19–24]. This geometry consists out of six square and eight hexagonal faces and is capable to partition the space into identical equal-volume units with minimal surface energy. However, we see that in this model all foam struts are identical, and the nodes, where the struts interconnect, are quite simplified. Although such Kelvin cell models have proven to be efcient and useful to model the mechanical response of cellular materials in the literature, the geometry of the Kelvin cell does not comply with a real foam topology. The cells of real foams are irregular polyhedra with anywhere from 9 to 17 faces when

Preprints (www.preprints.org) | NOT PEER-REVIEWED | Posted: 11 March 2022 doi:10.20944/preprints202203.0167.v1

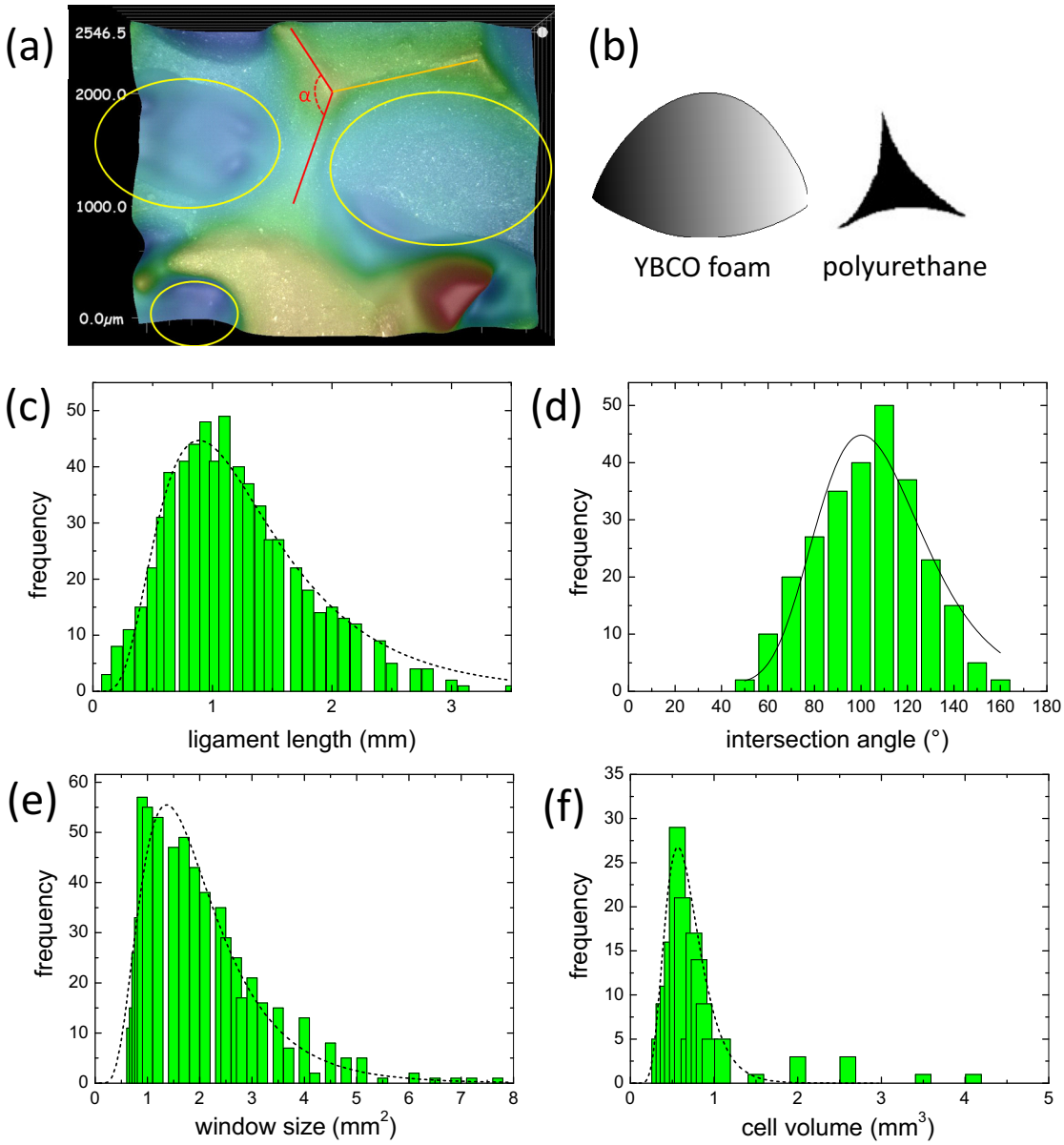

Figure 7. (**a**) Definitions of the ligament length (▬), the intersection angle α (▬) and the window size (yellow ellipses). (**b**) presents the typical cross section found by profile analysis for the YBCO foam (left) compared to the cross section found by Jang *et al.* [21]. (**c-f**) Statistical distribution analysis of the ligament (strut) lengths, the window size, the intersection angles and the cell size. The black dashed lines indicate log-normal fits to the data, and a normal fit in (**d**).

regarding nearly monodisperse foams. The material is concentrated in the nearly straight ligaments and in the nodes where they intersect. Therefore, the mechanical properties of foams depend strongly on the microstructure realized, and thus, on the basic properties of the base material used to prepare the foam sample.

The specific part of the microstructure, which is relevant for the mechanical properties of the foam, is the shape and geometry of the various nodes [21] as there is a large amount of material concentrated. Jang *et al.* showed further that the cross section of a ligament changes along its length, being relatively small in the center and growing towards the ends, which is due to an elongation when forming the polyurethane foam. For their polyurethane foam sample, they found a characteristic three-cusp hypocycloid cross section of Plateau borders, which is illustrated in Fig. 7 (b, right). From our present analysis, it is obvious that the flow of the liquid phase in the IG-process has altered the cross section of the foam struts or ligaments. The shape, as revealed by a large number of profiles taken from the optical

Preprints (www.preprints.org) | NOT PEER-REVIEWED | Posted: 11 March 2022 doi:10.20944/preprints202203.0167.v1

images, has changed to a paraboloid type (see Fig. 7 (b), left), and the sharp cusps of the original polyurethane foam have almost vanished. We further note that there is a spatial variation of the strut shape within the foam sample. From the bottom side, which was closest to the liquid source, the shape is found to change from the parabolic type (which contains more material on the ligands) to a more cusp-like type at the top face of the foam sample, which indicates the amount of liquid which was present during the processing. Previous work on flux pinning and critical currents in the foam sample [47,48] also revealed a clear dependence on the position within the original foam, and the TF measurements on all sides of a foam sample demonstrated that the top side was the weakest one [12]. Thus, this finding is another important issue for improving the properties of future YBCO foam samples.

Figures 7 (c)–(f) present the results of our image analysis. Figure 7 (c) gives the histogram of the ligament lengths from 601 ligaments, ranging between 0.12 and 3.5 mm. All data were fitted by log-normal functions (dashed black lines) with $y_0 = 0$. The resulting parameters are x_c =1.2 mm, $w = 0.55$ and $A = 53$. Similar to the data presented by Montmimy *et al.* [20], the data fall in a right-skewed distribution, which is common for natural systems. In Fig. 7 (d), the intersection angle histogram is presented, which represent a nearly normal distribution. The mean angle determined here is 104.1° (standard deviation 1.25°), which is smaller than the angle found by Montmimy *et al.* in their polyurethane foams, and clearly smaller than the tetrahedral angle of 109.5°. The foam window size distribution is shown in Fig. 7 (e), yielding $x_c = 1.25$ mm, $w = 0.26$ and $A = 35$. Like in the case of Montmimy *et al.*, this distribution is again right-skewed, but much stronger than the distribution of the ligament length, which says that there is a bigger variation of the window sizes as compared to the ligament lengths. Finally, Fig. 7 (f) gives the cell size histogram (155 cells analyzed) with the parameters $x_c = 0.84$ mm, $w = 0.12$ and $A = 8$. Altogether, this analysis demonstrates that the real foam structure is clearly different from a simple Kelvin cell, and the parameter set obtained will be useful for generating a true foam model. The important finding here is the fact that the cross sections of the YBCO foam are distinctly different from the polyurethane foam, and also from the intermediate Y-211 foam.

3.4. First modelling of field cooling and trapping

Finally, a first attempt to model the properties of a superconducting foam sample is presented here. The modelling was started using a Kelvin type model of a foam cell as depicted in Fig. 8 (a). The selected parameters are as follows: foam cell 5 mm wide, 0.25 mm thick struts, and the cell consists of circles with radius $b = 0.833$ mm and ellipses with major axis $a = 1.25$ mm and minor axis $b = 0.833$ mm. The foam is arbitrary tilted by 10° from the z-axis and 10° along the x-axis. A surface representing the field mapping area is placed at 2.75 mm above the foam. The calculations were done using classical **H** formulation coupled with circuit coupling or external field [49], or alternatively, using the **A-H** coupled formulation [50] implemented in the PDE module and the global equation module in COMSOL Multiphysics version 5.2a. The electrical parameters to simulate the YBCO foam sample use the power law $E(J) = E_c(J/J_c)^n$ with the parameters $E_c = 1\ \mu$V/cm, $n = 20$, and a critical current density $J_c = 1000$ A/mm^2, corresponding to the measurements on foam struts of Ref. [48]. Field cooling in a field of $B_{\mathrm{app}} = 50$ mT was modelled after reducing the field linearly towards 0 within 10 s, and the end of the process is depicted in Fig. 8 (b). Finally, a simulated trapped field distribution is presented in Fig. 8 (c), which gives a nearly homogeneous TF distribution.

The results of the TF modelling give already reasonable output as compared to the measured TF values in [12]. This is a first hint that a simple approach to model the superconducting performance of a foam sample is sufficient for most purposes. Introducing irregular cell sizes and a variation of the ligament thickness will not lead to higher calculated TF values, but may better reproduce the effects of current loop compression, etc. This will be a topic for future investigations. An interesting finding are the reddish areas along the foam struts as seen in Fig. 8 (b), depicting the field-cooled flux distribution. This

Preprints (www.preprints.org) | NOT PEER-REVIEWED | Posted: 11 March 2022 doi:10.20944/preprints202203.0167.v1

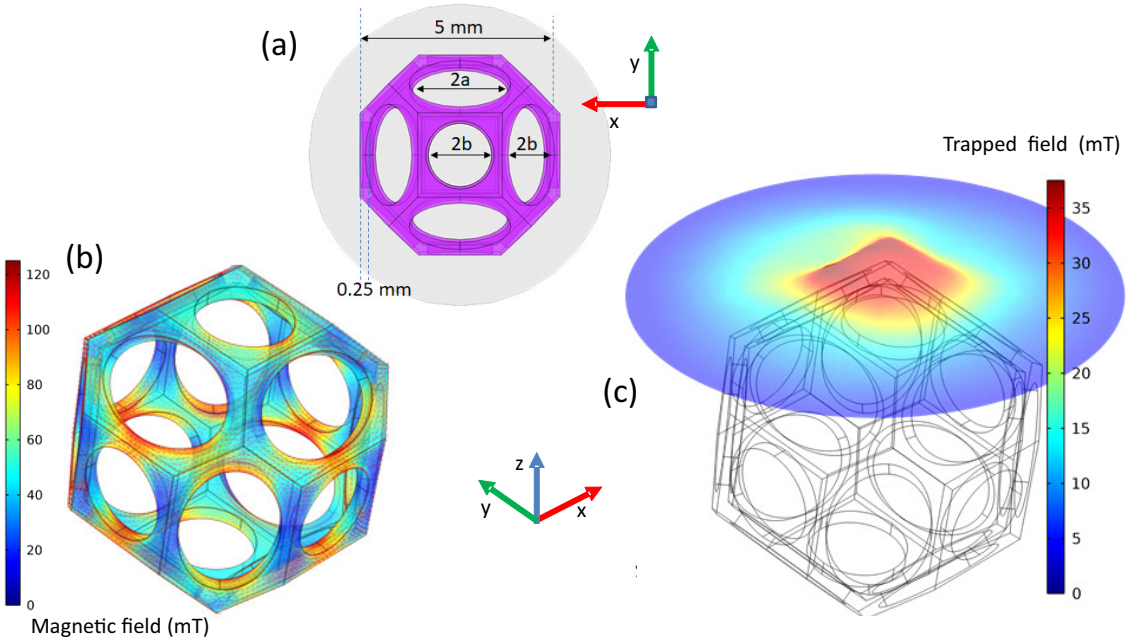

Figure 8. First modelling of trapped fields of a foam using the Kelvin cell, the dimensions of which are given in (**a**). (**b**) presents the distribution of the local magnetic field after field cooling in a field of 50 mT, and (**c**) gives the trapped field distribution at 2.75 mm above the foam.

observation implies that the thinnest sections of the foam ligaments form bottlenecks for the superconducting currents in the foam, experiencing the highest magnetic fields. Thus, the present shape of the foam ligaments is by no means well-suited for a high current density. Therefore, these first results point out that a more regular shape of the foam cells and, correspondingly, regular orientation of the foam ligaments would bring a better current distribution (as the main current flow takes place within the Cu-O-planes) in a superconducting foam sample. Such kind of structures could be produced by 3D printing/additive manufacturing as was already demonstrated in Refs. [51–53], which could significantly improve the TF performance of porous superconducting materials [54,55].

Regarding the very specific microstructure of the superconducting YBCO foams, one must note here that the foam struts of the superconducting foams have a different shape as compared to the starting polyurethane foams. Strongly linked to the capillary flow of the liquid phase during IG-processing, a specific microstructure of the superconducting foams results. Tiny Y-211 particles are located mostly in groove-like channels within the YBCO matrix [33], and the strut surface exhibits presence of $Ba_3Cu_5O_8$-particles stemming form the liquid source, which may also contribute to the flux pinning. Such additional particles on the sample surface were not seen previously in the commonly prepared bulk samples. All these details are essential for the superconducting performance of the foam samples. Thus, the final model of a superconducting foam must consider all these specific details of the foam microstructure.

4. Conclusions

A detailed analysis of the microstructure of superconducting YBCO foams revealed several interesting details, including the effects of the capillary flow of the liquid phase in the IG-process along the foam struts, the formation of $Ba_3Cu_5O_y$ particles and flow patterns on the internal surfaces of the foam and the formation of tiny Y-211 nanoparticles located in channel-like structures within the YBCO matrix. SEM and digital optical microscopy provide valuable input to better understand the real foam structure, revealing also clear differences to the polyurethane foams, which served as the base material. First modelling of the magnetic properties was done using the regular Kelvin cell approach and the **H**-formulation, which could already reproduce the basics of the trapped field measure-

Preprints (www.preprints.org) | NOT PEER-REVIEWED | Posted: 11 March 2022 doi:10.20944/preprints202203.0167.v1

ments. Furthermore, the model data suggest that an uniform distribution of cell sizes could provide better TF performance as the irregular structure of the present YBCO foam material.

The material of this manuscript was presented at the HTS modelling 2020 workshop, Nancy, held online in June, 22-23, 2021. This work is part of the SUPERFOAM international project funded by ANR and DFG under the references ANR-17-CE05-0030 and DFG-ANR Ko2323-10, respectively.

Author Contributions: Conceptualization, M.R.K.; Formal Analysis, M.R.K., A.K.-V., K.B., and D. G.; Investigation, M.R.K., A.K.-V., Q. N., G. H., and K. B.; funding acquisition: M.R.K. and K.B.; supervision, B. D.; Writing-Original Draft Preparation, M.R.K.; Writing-Review and Editing, M.R.K., A.K.-V., K.B., and D.G. All authors read and agreed to the published version of the manuscript.

Funding: This work is part of the SUPERFOAM international project funded by ANR and DFG under references ANR-17-CE05-0030 and DFG-ANR Ko2323-10, respectively.

Data Availability Statement: Datasets obtained and analyzed during the study are available from the corresponding authors on reasonable request.

Acknowledgments: We thank G. Schmitz (ACCESS, Aachen, Germany) for providing us the first foam sample and J. Schmauch (Saarland University) for technical assistance.

Conflicts of Interest: The authors declare no conflict of interest.

References

1. Reddy, E. S.; Schmitz, G. J. Superconducting foams. *Supercond. Sci. Technol.* **2002**, *15*, L21-L24; doi: 10.1088/0953-2048/15/8/101.
2. Reddy, E. S.; Schmitz, G. J. Ceramic foams. *Am. Ceram. Soc. Bull.* **2002**, *81*, 35-37.
3. Reddy, E. S.; Herweg, M.; Schmitz, G. J. Processing of Y_2BaCuO_5 foams. *Supercond. Sci. Technol.* **2003**, *16*, 608-612: doi: 10.1088/0953-2048/16/5/311.
4. Patel, A.; Giunchi, G.; Figini Albisetti, A.; Shi, Y.; Hopkins, S. C.; Palka, R.; Cardwell, D. A.; Glowacki, B. A. High Force Magnetic Levitation Using Magnetized Superconducting Bulks as a Field Source for Bearing Applications. *Phys. Proc.* **2012** *36*, 937-942; doi: 10.1016/j.phpro.2012.06.233.
5. Werfel, F. N.; Floegel-Delor, U.; Riedel, T.; Goebel, B.; Rothfeld, R.; Schirrmeister, P.; Wippich, D. Large-scale HTS bulks for magnetic application. *Physica C: Superconductivity* **2013** *484*, 6–11; doi: 10.1016/j.physc.2012.03.007.
6. Ogata, M.; Matsue, H.; Yamashita, T.; Hasegawa, H.; Nagashima, K.; Maeda, T.; Matsuoka, T.; Mukoyama, S.; Shimizu, H.; Horiuchi, S. Test equipment for a flywheel energy storage system using a magnetic bearing composed of superconducting coils and superconducting bulks. *Supercond. Sci. Technol.* **2016** *29*, 054002; doi: 10.1088/0953-2048/29/5/054002.
7. Durrell, J. H.; Ainslie, M. D.; Zhou, D.; Vanderbemden, P.; Bradshaw, T.; Speller, S.; Filipenko, M.; Cardwell, D. A. Bulk superconductors: A roadmap to applications. *Supercond. Sci. Technol.* **2018**, *31* 103501; doi: 10.1088/1361-6668/aad7ce.
8. Yang, W.; Liao, D.; Yao, L. Effects of magnetization conditions on dynamic characteristics of spacecrafts with superconducting flux pinning docking interfaces. *J. Appl. Phys.* **2018** *124*, 213901; doi: 10.1063/1.5047073.
9. Dorget, R.; Nouailhetas, Q.; Colle, A.; Berger, K.; Sudo, K.; Ayat, S.; Lévêque, J.; Koblischka, M. R.; Sakai, N.; Oka, T.; Douine, B. Review on the Use of Superconducting Bulks for Magnetic Screening in Electrical Machines for Aircraft Applications. *Materials* **2021**, *14*, 2847; doi: 10.3390/ma14112847.
10. Tang, R.; Song, Y.; He, J.; Liu, X.; Ren, Y.; Zhou, D.; Li, J.; Den, Z. Correlation Between Density and Levitation Performance of YBCO Bulk Superconductor Over Halbach NdFeB Guideway. *IEEE Trans. Appl. Supercond.* **2022** *32*, 3600504; doi: 10.1109/TASC.2021.3139576.
11. Noudem, J. G. Developing of shaping textured superconductors. *J. Supercond.* **2011**, *24*, 105-110; doi: 10.1007/s10948-010-0905-7.
12. Koblischka, M. R.; Pavan Kumar Naik, S.; Koblischka-Veneva, A.; Murakami, M.; Gohkfeld, D.; Reddy, E. S.; Schmitz, G. J. Superconducting YBCO foams as trapped field magnets. *Materials* **2019** *12*, 853; doi: 10.3390/ma12060853.
13. Bartolomé, E.; Granados, X.; Puig, T.; Obradors, X.; Reddy, E. S.; Schmitz, G. J. Critical state in superconducting single-crystalline $YBa_2Cu_3O_7$ foams: Local versus long-range currents. *Phys. Rev.* B **2004**, *70*, 144514; doi: 10.1103/PhysRevB.70.144514.
14. Carrera, M.; Amoros, J.; Carrillo, A. E.; Obradors, X.; Fontcuberta, J. Current distribution maps in large YBCO melt-textured blocks. *Physica C* **2003**, *385*, 539–543; doi: 10.1016/S0921-4534(02)02289-X.
15. Johansen, T. H. Flux-pinning-induced stress and magnetostriction in bulk superconductors. *Supercond. Sci. Technol.* **2000**, *13*, R121–R137; doi: 10.1088/0953-2048/13/10/201.
16. Yong, H.-D.; Zhou, Y.-E. Effect of nonsuperconducting particles on the effective magnetostriction of bulk superconductors. *J. Appl. Phys.* **2008** *104*, 043907; doi: 10.1063/1.2952042.
17. Diko, P. Cracking in melt-grown RE-Ba-Cu-O single-grain bulk superconductors. *Supercond. Sci. Technol.* **2004**, *17*, R45–R58; doi: 10.1088/0953-2048/17/11/R01.

Preprints (www.preprints.org) | NOT PEER-REVIEWED | Posted: 11 March 2022 doi:10.20944/preprints202203.0167.v1

18. Diko, P.; Chaud, X.; Antal, V.; Kaňuchová, M.; Šefčíková, M.; Šuster, D.; Kováč, J. Elimination of Oxygenation Cracking in YBCO Bulk Superconductors. *Key. Eng. Mater.* **2009** *409*, 216–222; doi: 10.4028/www.scientific.net/KEM.409.216.
19. Gibson, L. J.; Ashby, M. F. Cellular Solids: Structure and Properties 2nd ed., Cambridge University Press, Cambridge, U.K., 1999.
20. Montminy, M. D.; Tannenbaum, A. R.; Macosko, C. W. The 3D structure of real polymer foams. *J. Colloid Interface Sci.* **2004**, *280*, 202-211; doi:10.1016/j.jcis.2004.07.032.
21. Jang, W.-Y.; Kraynik, A. M.; Kyriakides, S. On the microstructure of open-cell foams and its effect on elastic properties. *Int. J. Solids Struct.* **2008**, *45*, 1845-1875; doi:10.1016/j.ijsolstr.2007.10.008.
22. Buffel, B.; Desplentere, F.; Bracke, K.; Verpoest, I. Modelling open cell-foams based on the Weaire–Phelan unit cell with a minimal surface energy approach. *Int. J. Solids Struct.* **2014**, *51*, 3461-3470; doi: 10.1016/j.ijsolstr.2014.06.017.
23. Nie, Zh.; Lin, Y.; Tong, Q. Modeling structures of open cell foams. *Comput. Mater. Sci.* **2017**, *131*, 160–169; doi: 10.1016/j.commatsci.2017.01.029.
24. Fanelli, P.; Evangelisti, A.; Salvini, P.; Vivio, F. Modelling and characterization of structural behaviour of Al open-cell foams. *Materials and Design* **2017**, *114*, 167-175; doi: 10.1016/j.matdes.2016.10.052.
25. Banhart, J. Manufacture, characterisation and application of cellular metals and metal foams. *Prog. Mater. Sci.* **2001** *46*, 559-632; doi: 10.1016/S0079-6425(00)00002-5.
26. Onck, P. R.; van Merkerk, R.; Raaijmakers, A.; de Hoss, R. Th. M. Fracture of open- and closed-cell metal foams. *J. Mater. Sci.* **2005** *40*, 5821–582; doi: 10.1007/s10853-005-4996-7.
27. Lefebvre, L.-P.; Banhart, J.; Dunand, D. C. Porous Metals and Metallic Foams: Current Status and Recent Developments. *Adv. Eng. Mater.* **2008** *10*, 775–787; doi: 10.1002/adem.200800241.
28. Kaya, A. C.; Fleck, C. Deformation behavior of open-cell stainless steel foams. *Mater. Sci. Eng. A* **2014** *615*, 447–456; doi: 10.1016/j.msea.2014.07.098.
29. A. Jung, A.; Wocker, M.; Chen, Z.; Seibert, H. Microtensile testing of open-cell metal foams – Experimental setup, micromechanical properties. *Materials and Design* **2015** *88*, 1021–1030; doi: 10.1016/j.matdes.2015.09.091.
30. A. Jung, A.; Diebels, S. Modelling of metal foams by a modified elastic law. *Mechanics of Materials* **2016** *101*, 61–70; doi: 10.1016/j.mechmat.2016.07.007.
31. Devendra Kumar, N.; Shi, Y.-H.; Cardwell, D. A. Fabrication of bulk (RE)BCO superconductors by the infiltration and growth process: past, present and future. In *Superconductivity Applications Today and Tomorrow*, ed. Muralidhar, M.; Nova Science Publishers: Commack, New York, USA, 2017, pp. 1–35.
32. Namburi, D. K.; Shi, Y.-H.; Cardwell, D. A. The processing and properties of bulk (RE)BCO high temperature superconductors: current status and future perspectives. *Supercond. Sci. Technol.* **2021**, *34*, 053002; doi: 10.1088/1361-6668/abde88.
33. Koblischka, M. R.; Koblischka-Veneva, A.; Reddy, E. S.; Schmitz, G. J. Analysis of the microstructure of superconducting YBCO foams by means of AFM and EBSD. *J. Adv. Ceram.* **2014**, *3*, 317-325; doi: 10.1007/s40145-014-0123-z.
34. Reddy, E. S.; Rajasekharan, T. Fabrication of textured $REBa_2Cu_3O_7/RE_2BaCuO_5$ (RE = Y, Gd) composites by inltration and growth of RE_2BaCuO_5 preforms by liquid phases. *Supercond. Sci. Technol.* **1998**, *11*, 523–534; doi: 10.1088/0953-2048/11/5/014.
35. Keyence Corp. Optical microscopes, https://www.keyence.com/products/microscope/digital-microscope/vhx-7000/, visited 31.01.2022.
36. Image J Image processing and analysis in Java. https://imagej.nih.gov/ij/index.html, visited 31.01.2022.
37. Horcas, I.; Fernández, R.; Gómez-Rodríguez, J. M.; Colchero, J.; Gómez-Herrero, J.; Baro, A. M. WSXM: A software for scanning probe microscopy and a tool for nanotechnology. *Rev. Sci. Instrum.* **2007**, *78*, 013705; doi: 10.1063/1.2432410.
38. TexSEM Laboratories (TSL) Orientation Imaging Microscopy Software V7.2, User Manual, TexSEM laboratories (TSL), Draper, UT, USA, 2015.
39. Reimer, L. *Scanning Electron Microscopy: Physics of Image Formation and Microanalysis.* Springer Science: Berlin, Heidelberg, Germany, 1985.
40. Koblischka, M. R.; Koblischka-Veneva, A. Applications of the electron backscatter diffraction technique to ceramic materials. *Phase Trans.* **2013**, *86*, 651-660; 10.1080/01411594.2012.726729.
41. A. Koblischka-Veneva et al., in preparation.
42. Guilmeau, E.; Lambert, S.; Chateigner, D.; Ouladdiaf, B.; Noudem, J.G. Quantitative texture analysis of polyphased oxides by diffraction: example of Bi2223 sinter-forged ceramic and Y123 foam superconductors. *Mat. Sci. Eng. B* **2003**, *104*, 107–112; doi:10.1016/S0921-5107(03)00180-6.
43. Noudem, J.G.; Guilmeau, E.; Chateigner, D.; Lambert, S.; Reddy, E. S.; Ouladdiaf, B.; Schmitz, G. J. Properties of $YBa_2Cu_3O_y$-textured superconductor foams. *Physica C* **2004**, *408–410*, 655–656; doi:10.1016/j.physc.2004.03.098.
44. Koblischka-Veneva, A.; Koblischka, M. R.; Schmauch, J.; Murakami, M. Secondary phase particles in bulk, infiltration-growth processed YBCO investigated by transmission Kikuchi diffraction and TEM. *Supercond. Sci. Technol.* **2020**, *33*, 034010, doi: 10.1088/1361-6668/ab6ebf.
45. Koblischka-Veneva, A.; Koblischka, M. R.; Ide, N.; Inoue, K.; Muralidhar, M.; Hauet, T.; Murakami, M. Microstructural and magnetic analysis of a superconducting foam and comparison with IG-processed bulk samples *J. Phys. Conf. Ser.* **2016**, *695*, 012002: doi: 10.1088/1742-6596/695/1/012002.
46. Koblischka, M. R.; Pavan Kumar Naik, S.; Koblischka-Veneva, A.; Gokhfeld, D.; Murakami, M. Flux creep after field trapping in $YBa_2Cu_3O_y$ foams. *Supercond. Sci. Technol.* **2020**, *33*, 044008; doi: 10.1088/1361-6668/ab72c3.

Preprints (www.preprints.org) | NOT PEER-REVIEWED | Posted: 11 March 2022 doi:10.20944/preprints202203.0167.v1

47. Koblischka, M. R.; Koblischka-Veneva, A.; Berger, K.; Nouailhetas, Q-; Douine, B.; Reddy, E. S.; Schmitz, G. J. Current flow and flux pinning properties of YBCO foam struts. *IEEE Trans. Appl. Supercond.* **2019**, *29*, 8001405; doi: 10.1109/TASC.2019.2894712.
48. Koblischka, M. R.; Koblischka-Veneva, A.; Chang, C.; Hauet, T.; Reddy, E. S.; Schmitz, G. J. Flux pinning analysis of superconducting YBCO foam struts. *IEEE Trans. Appl. Supercond.* **2019**, *29*, 8001905; doi: 10.1109/TASC.2018.2880334.
49. Kapek, J.; Berger, K.; Koblischka, M. R.; Trillaud, F.; Lévêque, J. 2-D Numerical Modeling of a Bulk HTS Magnetization Based on H Formulation Coupled With Electrical Circuit. *IEEE Trans. Appl. Supercond.* **2019**, *29*, 6801405; doi: 10.1109/TASC.2019.2897331.
50. Kapek, J.; Berger, K.; Lévêque, J. 2D and 3D validation of a hybrid method based on A and H formulations for Pulsed Field Magnetization. 7th International Workshop on Numerical Modelling of High Temperature Superconductors (HTS 2020), 2021; https://hal.univ-lorraine.fr/HTS2020/hal-03273940v1.
51. Wei, X.; Nagarajan, R. S.; Peng, E.; Xue, J.; Wang, J.; Ding, J. Fabrication of $YBa_2Cu_3O_{7-x}$ (YBCO) superconductor bulk structures by extrusion freeforming. *Ceram. Int.* **2016**, *42*, 15836-15842; doi: 10.1016/j.ceramint.2016.07.052
52. Zhang, B.; Zhang, Q.; He, P.; Ma, Y.; Shen, L.; Zhang, X.; Zhou, Y. Efficient Fabrication of Ultralight $YBa_2Cu_3O_{7-x}$ Superconductors with Programmable Shape and Structure. *Adv. Funct. Mater.* **2021**, *31*, 2100680; doi: 10.1002/adfm.202100680.
53. Mendes, D.; Sousa, D.; Cerdeira, A. C.; Pereira, L. C. J.; Marques, A.; Murta-Pina, J.; Pronto, A.; Ferreira, I. Low-cost and high-performance 3D printed YBCO superconductors. *Ceram. Int.* **2021**, *47* 381-387; doi: 10.1016/j.ceramint.2020.08.143.
54. Koblischka, M. R.; Koblischka-Veneva, A. Porous high-T_c superconductors and their applications. *AIMS Material Sci.* **2018**, *5*, 1199-1213; doi: 10.3934/matersci.2018.6.1199.
55. Gokhfeld, D.; Koblischka, M. R.; Koblischka-Veneva, A., ВЫСОКОПОРИСТЫЕ СВЕРХПРОВОДНИКИ: СИНТЕЗ, ИССЛЕДОВАНИЯ И ПЕРСПЕКТИВЫ. *Fizikia Metalov i Metalovidenie* **2020**, *121*, 1026-1038 (in Russian); Gokhfeld, D.; Koblischka, M. R.; Koblischka-Veneva, A., Highly Porous Superconductors: Synthesis, Research, and Prospects. *Physics of Metals and Metallography* **2020**, *121*, 936–948 (English translation); doi:10.1134/S0031918X20100051.